5

Metal-oxide Nanowires by Thermal Oxidation Reaction Technique

Supab Choopun, Niyom Hongsith and Ekasiddh Wongrat
Department of Physics and Materials Science, Faculty of Science, Chiang Mai University Chiang Mai 50200 and ThEP Center, CHE, Bangkok 10400, Thailand

1. Introduction

The metal-oxides are very interesting materials because they possess wide and universal properties including physical and chemical properties. For example, metal-oxides exhibit wide range of electrical property from superconducting, metallic, semiconducting, to insulating properties (Henrich & Cox, 1994). The wide ranges of properties makes metal-oxide suitable for many applications including corrosion protection, catalysis, fuel cells, gas sensor, solar cells, field effect transistor, magnetic storage (Henrich, 2001), UV light emitters, detectors, piezoelectric transducers, and transparent electronics (Hsueh & Hsu, 2008) etc.

Recently, nanostructures of metal-oxide such as nanowire, nanorod, nanobelt, nanosheet, nanoribbon, and nanotube have gained a great attention due to their distinctive and novel properties from conventional bulk and thin film materials for new potential applications. These unique properties cause by quantum confinement effect (Manmeet et al., 2006), lower dimensionality (Wang et al., 2008), change of density of state (Lyu et al., 2002), and high surface-to-volume ratio (Wangrat et al., 2009).

Nanowires can be regarded as one-dimensional (1D) nanostructures which have gained interest for nanodevice design and fabrication (Wang et al., 2008). As an example of metal-oxide nanowires, the materials are focused on zinc oxide (ZnO) and copper oxide (CuO). ZnO which is n-type semiconductor has been widely studied since 1935 with a direct band gap of 3.4 eV and large exciton binding energy of 60 meV at the room temperature (Coleman & Jagadish, 2006). ZnO has a wurtzite structure, while CuO, which is p-type semiconductor with narrow band gap of 1.2 eV , has a monoclinic crystal structure (Raksa et al., 2009).

ZnO and CuO can be synthesized by various techniques such as pulse laser deposition (PLD) (Choopun et al., 2005), chemical vapor deposition (VD) (Hirate et al., 2005), thermal evaporation (Jie et al., 2004; Ronning et al., 2004), metal-catalyzed molecular beam epitaxy (MBE) (Wu et al., 2002; Chan et al., 2003; Schubert et al., 2004), chemical beam epitaxy (CBE) (Björk et al., 2002) and thermal oxidation technique (Wongrat et al., 2009). Thermal oxidation technique is interesting because it is a simple, and cheap technique. Many researchers have reported about the growth of ZnO and CuO by thermal oxidation technique with difference conditions such as temperature, time, catalyst, and gas flow. The list of metal-oxide nanowires synthesized by thermal oxidation is shown in Table 1.

Source: Nanowires, Book edited by: Paola Prete,
ISBN 978-953-7619-79-4, pp. 414, March 2010, INTECH, Croatia, downloaded from SCIYO.COM

Materials	Temperature (°C)	Oxidation Time	Morphology	Diameter (nm)	Growth direction	Ref.
CuO	400-700	2-4 h	nanowire	30-100	$[\bar{1}11]$ and $[111]$	(Jiang et al., 2002)
CuO	300-500	0.5-24 h	nanowire	500	-	(Chen et al., 2008)
CuO	600	6 h	nanowire	100-400	[110]	(Raksa et al., 2008)
CuO	400	2 h	nanowire	60	$[\bar{1}11]$	(Nguyen et al., 2009)
CuO	400	4 h	nanowire	40-100	-	(Zeng et al., 2009)
CuO	400-800	4 h	nanowire	50-100	[010]	(Manmeet et al., 2006)
CuO	500	1.5 h	nanowire	100	$[\bar{1}11]$	(Hansen et al., 2008)
ZnO	300	5 min	Nanowire and nanoflake	100-150	-	(Hsueh & Hsu, 2008)
ZnO	600	24 h	nanowire	100-500	-	(Wongrat et al., 2009)
ZnO	300-600	1 h	nanoneedle	20-80	[0001]	(Yu & Pan, 2009)
ZnO	500	1 h	nanoplate	200-600	$[11\bar{2}0]$	(Kim et al., 2004)
ZnO	200-500	30 min	nanowire	30-350	[0001]	(Schroeder et al., 2009)
ZnO	300-600	1 h	nanowire	12-52	$[11\bar{2}0]$	(Fan et al., 2004)
ZnO	< 400	30 min	nanowire	20-150	$[11\bar{2}0]$	(Ren et al., 2007)
ZnO	600	1.5 h	nanowire	30-60	[0001]	(Sekar et al., 2005)
ZnO	400-600	1 h	nanowire and nanorod	20	$[2\bar{1}\bar{1}0]$	(Liang et al., 2008)

Table 1. List of metal-oxide nanowires synthesized by thermal oxidation.

2. Oxidation reaction

The thermal oxidation technique can be used to fabricate nanowires that are low-cost and high quality. A growth condition can be controlled with difference temperature and time. The oxidation reaction of metal on the surface yields metal-oxide semiconductor. However, the metal-oxide may be bulk or nanosize depending on the growth conditions such as the temperature, time, metal-catalyst and gas atmosphere.

In our previous report, we have successful synthesized ZnO and CuO nanowires by thermal oxidation technique without metal-catalyst under normal atmosphere. Zn metal was screened on the alumina substrate and sintered at the temperature of 500-700°c for 24 hours. It was found that the oxidation reaction occurred with two mechanism; above melting point of Zn metal and lower melting point of Zn metal. In phase diagram as shown in Fig. 1, Zn in liquid phase forms to ZnO nanowires at temperature more than 419.6°c while less than 419.6°c Zn solid phase can be oxidized to form ZnO nanowires on the substrate. The oxidation reaction of Zn solid (below melting point) can be expressed as:

$$Zn(s)+\frac{1}{2}O_2(g)\rightarrow ZnO(s) \quad (1)$$

While the chemical reaction of Zn liquid is shown as:

$$Zn(l)+\frac{1}{2}O_2(g)\rightarrow ZnO(s) \quad (2)$$

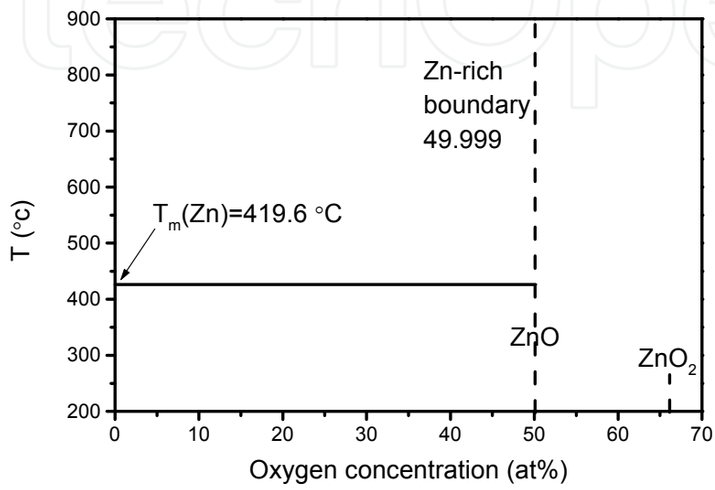

Fig. 1. Phase diagram of Zinc-Oxygen at the difference temperature (Ellmer & Klein, 2008).

Many researchers including us have reported about the synthesis of nanowires by thermal oxidation techniques. The mechanism of metal oxidation has also been reported by Wagner (Wagner & Grunewald, 1938). The oxide growth rate depends on transport properties such as diffusion coefficient that can be proved from Fick's first law at the steady state as following:

$$J=-D\frac{\partial c}{\partial x} \quad (1)$$

where J is the concentration gradient, c is the concentration of oxygen, D is the diffusion coefficient and x is the displacement. Integrating Eq. (1) when J/D is constant and the boundary conditions are given as

$$c(x=0,t)=c_1;\, c(x=T,t)=c_2 \quad (2)$$

, we get:

$$-\frac{JT}{D}=(c_2-c_1) \quad (3)$$

where c_2 is concentration in the interface regions of oxide-oxygen molecule, while c_1 is in regions of metal-oxide interface as shown in Fig 2.

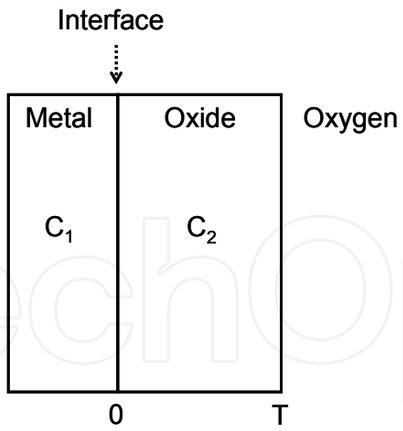

Fig. 2. Schematic diagram of metal-oxide interface and oxide-gas.

we assume c_1 is negligible since the number of oxygen is tiny. Therefore, Eq. (3) can be reduced to the following

$$-\frac{JT}{D} = c_2 \tag{4}$$

For conservation of mass (Belousov, 2007), Fick' s first law is indicated as:

$$J = c^* \frac{dT}{dt} \tag{5}$$

where c^* is the oxygen concentration in the oxygen product. From Eq. (4) and Eq. (5), we get

$$J = c^* \frac{dT}{dt} = -\frac{c_2 D}{T} \tag{6}$$

Integrating equation (6), the solution is formed as

$$T^2 = \frac{2c_2 Dt}{c^*} \tag{7}$$

where

$$k = \frac{2c_2 D}{c^*} \tag{8}$$

is a parabolic rate constant. From Eq. (7), it was found that the oxide thickness is proportional to the square root of time. However, parabolic rate constant is different for various metal-oxides since the diffusion in oxidation reaction is caused by many mechanisms such as metal vacancy, oxygen vacancy, metal interstitial and oxygen interstitial.

First, the oxidation reaction of metal occurs at the surface where metal lose electron to form M^{++} ions. Then, the electron from metal moves to the surface. The oxygen molecule and the electron reacts to form adsorbed oxygen (oxygen ion) on the surface. The adsorbed oxygen ions include O^{2-}, O^- and O_2^- which has reaction as (Martin & Fromm, 1997)

$$\left.\begin{aligned} \frac{1}{2}O_2 + 2e &\rightarrow O^{2-} \\ O_2 + e &\rightarrow O_2^- \\ \frac{1}{2}O_2 + e &\rightarrow O^- \end{aligned}\right\} \quad (9)$$

The diffusion across oxide layer owing to metal ion or oxygen ion is depended on the domination of transport. The transportation of ions can be considered for four possible mechanisms as shown in Fig. 3. First, the transportation of ions by oxygen is due to interstitial mechanism that the oxygen ions are more mobile than metal ions and pass from one interstitial site to one of its nearest-neighbor interstitial site without permanently displacing any of the matrix atom (Shewmon, 1989). Therefore, the new metal-oxide is formed at the metal-oxide interface as seen in Fig. 3(a). Second, if there is the vacancy of oxygen in the matrix atom or called unoccupied site (Shewmon, 1989), the nearest-neighbor oxygen ions can move from one to vacancy. The new metal-oxide is also formed at the metal-oxide interface as in Fig. 3(b).

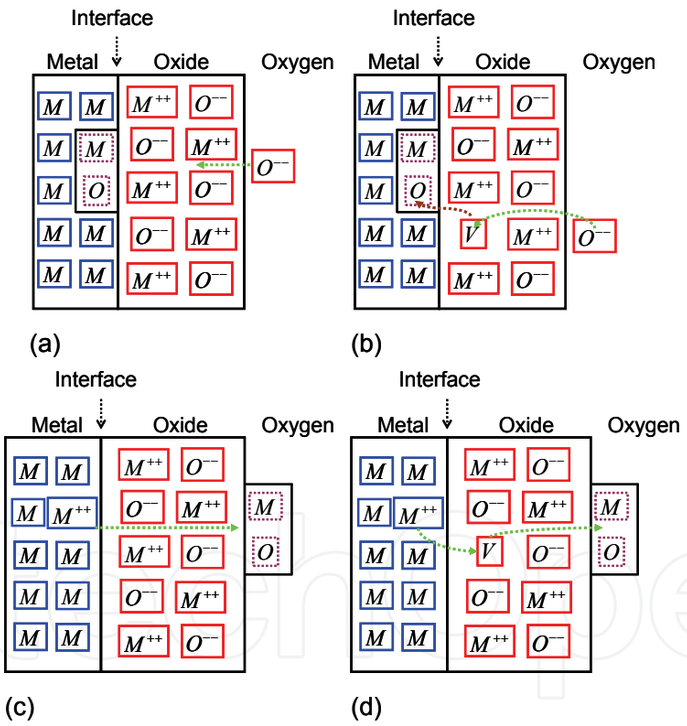

Fig. 3. Schematic diagrams of four possible mechanisms of ion transport in oxidation reaction, (a) the transportation of oxygen ions by oxygen interstitial mechanism (b) the transportation of oxygen ions by oxygen vacancy mechanism (c) the transportation of metal ions by metal interstitial mechanism (d) the transportation of metal ions by metal vacancy mechanism.

Third, on the contrary, it is for the case that the metal ions are more mobile than oxygen ions and pass from one site to the nearest-neighbor site without permanently displacing any of the matrix atom (Shewmon, 1989). The new metal-oxide is formed at oxide-oxygen interface as in Fig. 3 (c). Fourth, for the case that it has the unoccupied site of metal ions on the lattice,

the metal ions can jump from one to the nearest-neighbor unoccupied site. The new metal-oxide is also formed at the oxide-oxygen interface as in Fig. 3(d). The new metal-oxide in Fig. 3 (a) and (b) is in MO form, while in Fig. 3 (c) and (d) is in M_2O form (Martin & Fromm, 1997). Moreover, the oxidation reaction of metal forms two layers of oxide and metal. The ratio of molar volume of oxide to molar volume of metal called "Pilling-Bedworth ratio" which is the indicator of whether an oxide layer is protective. The Pilling-Bedworth ratio can be written by (Barsoum, 2003):

$$P-B\,ratio=\chi=\frac{V_{MO_{Z/2}}}{V_M}=\frac{MW_{MO_{Z/2}}\rho_M}{MW_M\rho_{MO_{Z/2}}} \tag{10}$$

where V_M, $V_{MOz/2}$ is the molar volume of the metal and of the metal-oxide, respectively. MW and ρ is the molecular weights and densities of the metal and oxide, respectively. For metals having a P-B ratio less than unity, the metal-oxide tends to be porous and unprotective because metal-oxide volume is not enough to cover the underlying metal surface. For ratios larger than unity, compressive stresses build up in the film, and if the mismatch is too large, (P-B ratio>2), the oxide coating tends to buckle and flake off, continually exposing fresh metal, and is thus nonprotective. The ideal P-B ratio is 1, but protective coatings normally form for metals having P-B ratios between 1 and 2 (Barsoum, 2003).

3. Gibb free energy

From the chemical oxidation reaction of metal, the two possible chemical reactions are

$$M(s)+\frac{1}{2}O_2(g)\rightarrow MO(s) \tag{11}$$

and

$$M(l)+\frac{1}{2}O_2(g)\rightarrow MO(s) \tag{12}$$

where M is defined by metal. The difference between the two chemical reactions is that metal solid can be formed by oxidation reaction process under a melting point while metal liquid can be formed above melting point. However, both reactions are spontaneous reactions. An important parameter to obtain physical insight into the materials aspect of thermodynamics potential is Gibb free energy. This section will be described about the Gibb free energy in term of thermodynamic parameter. The Gibb free energy of a phase is given by:

$$G=H-TS \tag{13}$$

In thermodynamics, the parameters such as enthalpy, entropy and Gibb free energy are normally absolute value. So, it can be identified by a relative value with convention at standard state. The standard state is assigned to compare with the reference state at pressure of 1 atm and 298 K. Firstly, the enthalpy of chemical reaction is typically described by the change of two state; initial state and final state. So, the enthalpy of compound in chemical reaction at standard state is simply given by:

$$\Delta H^0=\sum\Delta H^0_{products}-\sum\Delta H^0_{reac\,tants} \tag{14}$$

$$\Delta H^0 = \sum \Delta H^0_{MO} - \frac{1}{2}\sum \Delta H^0_{O_2} - \sum \Delta H^0_{M} \tag{15}$$

Similarly, entropy changes in chemical reactions can be obtained in a same way and the sum of standard entropy for chemical reaction can be written as:

$$\Delta S^0 = \sum \Delta S^0_{products} - \sum \Delta S^0_{reac\,tan\,ts} \tag{16}$$

$$\Delta S^0 = \sum \Delta S^0_{MO} - \frac{1}{2}\sum \Delta S^0_{O_2} - \sum \Delta S^0_{M} \tag{17}$$

Since, Gibb free energy is defined by Eq. (13), the Gibb free energy of chemical reaction process at various temperatures is given as:

$$\Delta G^0 = \Delta H^0 - T\Delta S^0 \tag{18}$$

On the other hand, if standard Gibb free energy is known, it can be simply calculated by:

$$\Delta G^0 = \sum \Delta G^0_{products} - \sum \Delta G^0_{reac\,tan\,ts} \tag{19}$$

4. Thermodynamics equilibrium

Typically, equilibrium system is a stable system with time and the certain properties of the system are uniform throughout with the same temperature and pressure. The various phases can co-exist without driving force. The variation of Gibb free energy through temperature and pressure can be indicated as

$$dG = -SdT + VdP \tag{20}$$

For a system undergo a process at constant temperature, Eq. (20) becomes:

$$dG = VdP \tag{21}$$

The surrounding oxygen, which is assumed to be ideal gas can react with metal to form metal-oxide. Eq. (21) can be rewritten as

$$dG = \frac{RT}{P}dP \tag{22}$$

Integrating between state 1 and 2,

$$\Delta G = RT\ln\frac{P_2}{P_1} \tag{23}$$

Since the reference state is 1 atm and 298 K, Eq. (23) is reduced as following:

$$G = G^0 + RT\ln P \tag{24}$$

It was found that Eq. (24) of Gibb free energy is a function of pressure and temperature. However, the system is not ideal system that the relation in Eq. (24) is non-linear. Thus, for real gas the new function of fugacity (f) is introduced and defined as:

$$dG = RTd\ln f \tag{25}$$

Integrating Eq. (25) with initial state and final state yields:

$$\Delta G = RT\ln\frac{f_2}{f_1} \tag{26}$$

The activity is defined by:

$$a = \frac{f}{f^0} \tag{27}$$

where f^0 is fugacity in standard state. Replacing Eq. (26) with Eq. (27)

$$\left.\begin{aligned} G - G^0 &= RT\ln a \\ G &= G^0 + RT\ln a \end{aligned}\right\} \tag{28}$$

From the chemical oxidation reaction of metal, the Gibb free energy in the system can be written by:

$$\Delta G = G_{MO} - G_M - \frac{1}{2}G_{O_2} \tag{29}$$

Substituting Eq. (28) to Eq. (29):

$$\Delta G = \left(G^0_{MO} + RT\ln a_{MO}\right) - \left(G^0_M + RT\ln a_O\right) - \frac{1}{2}\left(G^0_{O_2} + RT\ln a_{O2}\right) \tag{30}$$

when

$$\Delta G^0 = G^0_{MO} - G^0_M - \frac{1}{2}G^0_{O_2} \tag{31}$$

Eq. (30) can be given as:

$$\Delta G = \Delta G^0 + RT\ln\frac{a_{MO}}{a_M a_{O_2}^{1/2}} \tag{32}$$

The activity is approximately one in solid. While activity in oxygen is an oxygen pressure in the system so Eq. (32) can be reduced to:

$$\Delta G = \Delta G^0 - \frac{1}{2}RT\ln P_{O_2} \tag{33}$$

The important parameter from Eq. (33) is Gibb free energy at standard state which is the function of temperature and pressure. The kinetic of oxide nucleation to form the nanostructure depend on the diffusion of oxygen ions and metal ions which is determined by the change of Gibb free energy. Nevertheless, the simple method to consider oxidation reaction at various temperature and pressure can be performed by Ellingham diagram that will be discussed in the next section.

5. Ellingham diagram

The oxidation reaction of metal is related to temperature and pressure in Eq. (33). Ellingham have presented a simple method to consider oxidation reaction. The temperature and pressure can oxidize metal to form oxide layer at the equilibrium of oxygen, metal, and metal-oxide (ΔG=0). At the equilibrium, Eq. (33) can be reduced to:

$$\Delta G^0 = \frac{1}{2} RT \ln P_{O_2} \tag{34}$$

For 1 mole of oxygen molecule in chemical oxidation reaction, Eq. (33) turns to

$$\Delta G^0 = RT \ln P_{O_2} \tag{35}$$

The relation between Gibb free energy, temperature and the pressure of oxygen can be plotted in Fig. 4. The linear relation between Gibb free energy and temperature for chemical reaction of Cu to Cu_2O and CuO is plotted together in Fig. 4. This linear relation passes zero point of Gibb free energy at absolute zero temperature with slope of $RlnP_{O2}$. An intersection between two lines shows the equilibrium between Cu and Cu_2O at the pressure and temperature that can form metal-oxide. For example, Ellingham diagram for some metal oxidation reaction is given in Fig. 5. for given control pressure and temperature.

6. Metal-oxide nanowires by thermal oxidation reaction technique

Metal-oxide nanowires have been successfully synthesized by thermal oxidation technique. This technique has been successfully used for synthesizing ZnO or CuO by simply heating

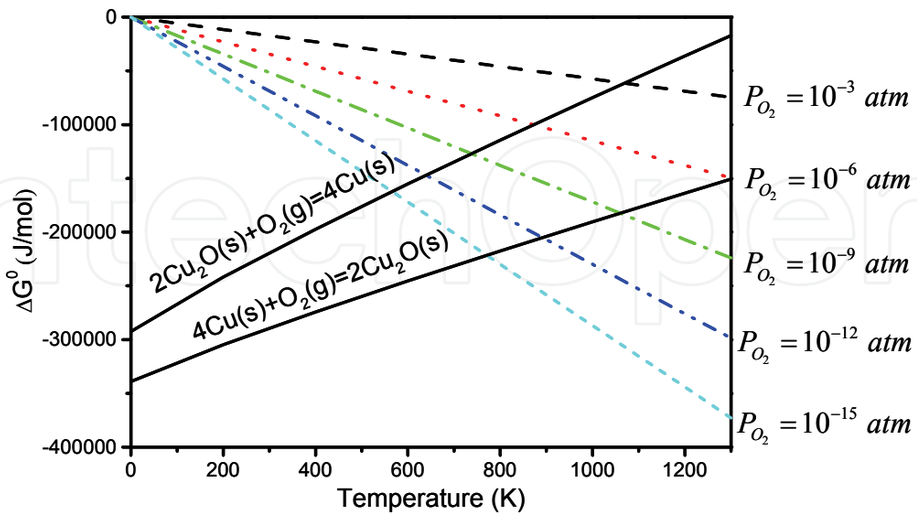

Fig. 4. Superposition between ΔG^0 versus T for oxidation reaction and for oxygen pressure at $\Delta G^0 = RT \ln P_{O_2}$.

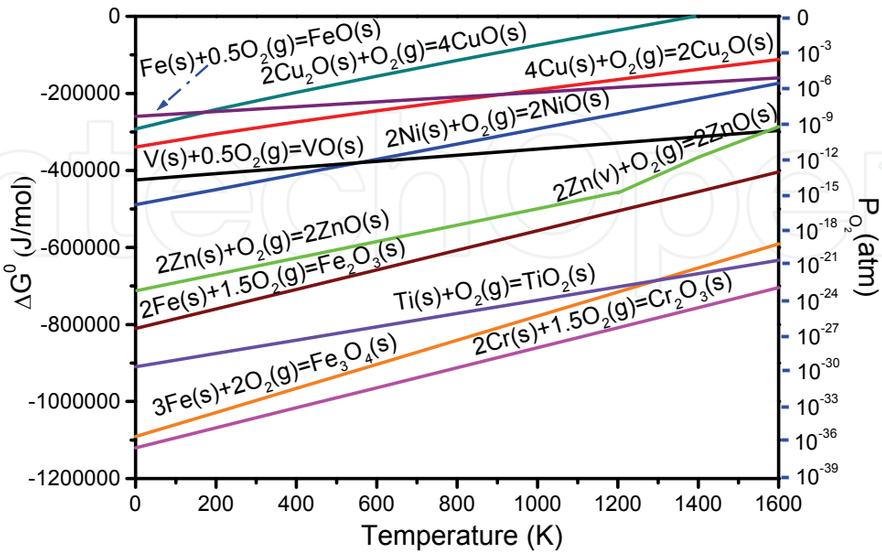

Fig. 5. Ellingham diagram for some metal-oxide.

pure Zn and Cu material sources, respectively. The process is usually conducted in a cylindrical furnace. The morphology of ZnO nanowires and CuO nanowires by thermal oxidation reaction technique revealed by field emission scanning electron microscopy (FE-SEM) are shown in Fig. 6 (a) and (b), respectively. ZnO nanowires were performed by heating zinc powder (purity 99.9%) that was screened on the alumina substrate. The oxidation process was sintered in a horizontal furnace in alumina crucible in air at atmospheric pressure at temperature 600°C for 24 hr. The ZnO nanowires have the diameters ranging from 60-180 nm and the lengths ranging from 5-10 μm. The wire-like structure of ZnO is clearly observed from TEM image, and the associative selected area electron diffraction pattern (SADP) as shown in Fig. 6 (c). The SADP shows a spot pattern, indicating a singlecrystalline property of the nanowire corresponding to the hexagonal structure of ZnO with the lattice constants, $a = b = 3.2$ Å, $c = 5.2$ Å. From the trace analysis,, it was found that the ZnO nanowire grew along the $< \bar{2}110 >$ direction on (0001) plane..

Likewise, CuO nanowires were performed by heating copper plate (~99% of purity) at temperature 600°C for 24 hr. Clearly, the oxidized products exhibited nanowire structure with the diameter ranging from 100–300 nm and the length from 10-50 μm. In addition, at higher heating temperature leads to larger diameter of nanowires. Fig. 6 (d) shows TEM bright field image of CuO nanowires with its associated SADP. The wire-like structure can be observed from TEM image. The SADP of the nanowire shows a spot pattern, indicating a single-crystalline property of the nanowire which corresponds to the monoclinic structure of CuO with the lattice constants, $a = 4.7$ Å, $b = 3.4$ Å and $c = 5.1$ Å, and from the trace analysis, the spots can be also confirmed that the growth direction of CuO nanowires is <110>.

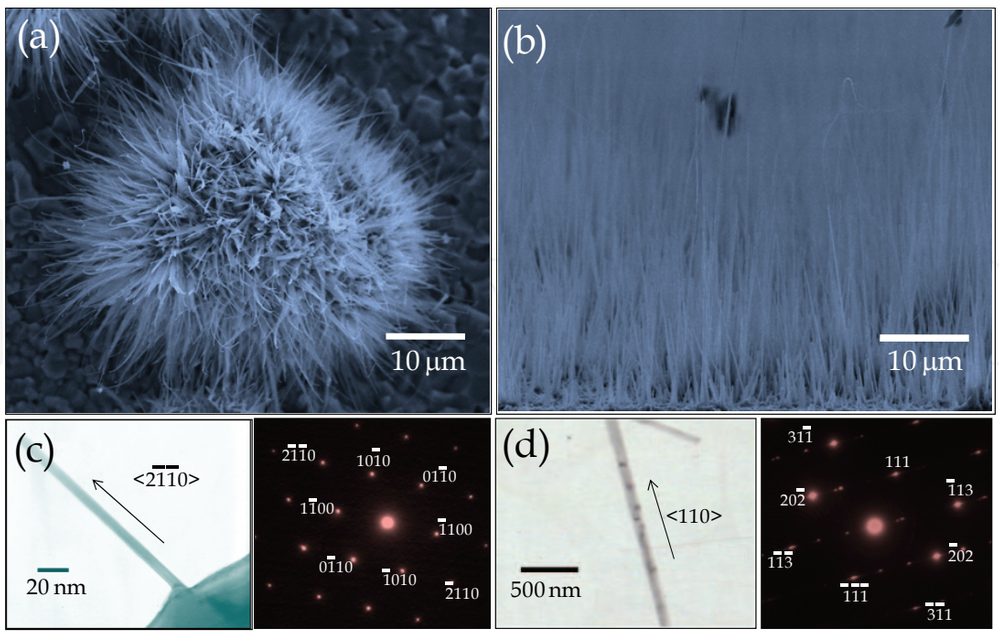

Fig. 6. FE-SEM images of (a) ZnO nanowires and (b) CuO nanowires, which prepared by thermal oxidation technique and TEM bright field image with the associated SADP for (c) ZnO nanowires and (d) CuO nanowires, respectively.

7. Growth mechanism of metal-oxide nanowire

Understanding the growth mechanism is critical in controlling and designing nanostructures. In 1950-1960, the growth mechanism of whisker that can be considered as a wire in micrometer size had been widely studied. V-S growth mechanism, V-L-S growth mechanism, and Frank dislocation growth mechanism were proposed for whisker growth (Dai, et al., 2003). However, the growth mechanism of metal-oxide nanowire should be different from whisker growth mechanism. Thus, in this section, we have proposed a possible growth mechanism that may be occurred in the formation of nanowire. The growth mechanism can be explained in term of Gibb free energy of oxidization process.

The growth mechanism of metal-oxide nanowire is proposed as in the following four steps: 1. oxygen adsorption, 2. surface oxidization to form nuclei, 3. nuclei arrangement and 4. nanowire formation as shown in Fig. 8.

Step 1. **oxygen adsorption:** Typically, oxygen molecules in air are adsorbed on the metal surface with diffusion process as described in Section 2. There are many reports to describe the mechanism of O_2 interaction with the transition metal surface (Martin & Fromm, 1997).

Step 2. **surface oxidization to form nuclei:** the metal-oxide nucleation was formed by diffusion of metal ions and/or oxygen ions in the oxide layer, and the reactions of metal ions with oxygen ions to form metal-oxide as seen in section 2.

To form nuclei of metal-oxide in the oxide layer (as in Fig. 7), metal-oxide nucleus is formed by agglomeration between metal ion and oxygen ion due to the minimization of surface energy. This phenomenon is similar to the coalescence behavior of two droplet of water when they are connected and then forming bigger

one droplet instead of staying separately. In order to explain the growth mechanism, Gibb free energy change per nucleus (not per mole) of metal-oxide with radius r and volume V is introduced and defined as

$$\Delta G_N = V\Delta G^0 + A_f\gamma_f \tag{36}$$

where A_f and γ_f is surface area and surface energy, respectively. For a given ΔG^0 which is usually negative, the magnitude of ΔG_N depends on only two terms: a volume energy and surface energy. Volume energy is propotional to $-r^3$, but surface energy is propotional to r^2. Thus, ΔG_N as a function of r exhibits maximum value at some critical radius, r^*, as seen in Fig. 7 (c).

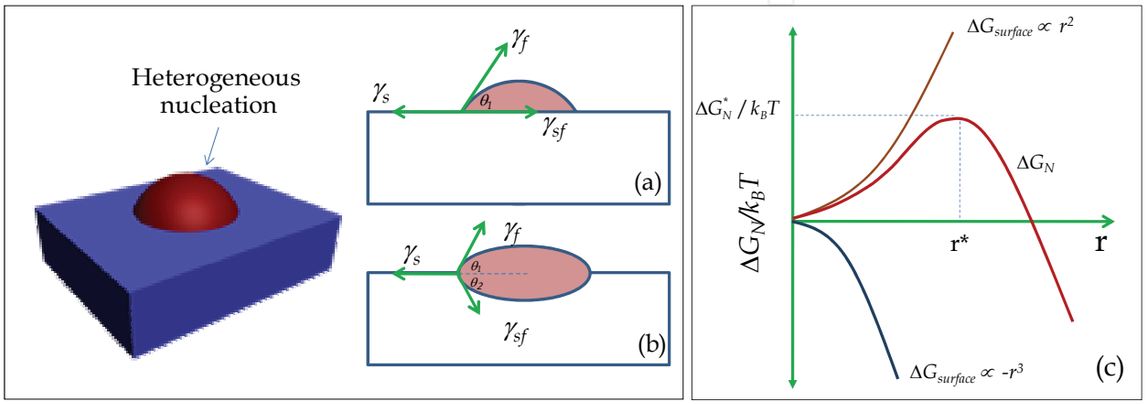

Fig. 7. Model of the metal-oxide nucleaion for (a) non-reactive and (b) reactive nucleation and (c) plot of ΔG_N as a function of radius.

For example in spherical homogeneous nucleation, the critical radius, r^*, can be simply obtained at $d(\Delta G_N/dr) = 0$ and can be written as

$$r^* = \frac{-2\gamma_f}{\Delta G^0} \text{ and } \Delta G_N^* = \frac{(16/3)\pi\gamma_f^3}{(\Delta G^0)^2} \tag{37}$$

Moreover, critical radius also implies the stability of nucleation. The nucleation will be stable at radius more than critical radius and proceed to grow spontaneously. In the other word, the spherical nucleation of stable phase forms with radius r when it can overcome the maximum energy barrier, ΔG^*_N or $\Delta G_N(r^*)$. However, the nucleation shape by oxidation process is different from spherical shape. Normally, nucleation shape by oxidation process is likely to be two shapes of nucleation: non-reactive and reactive nucleation as shown in Fig. 7 (a) and (b). The non-reactive reactive nucleation are metal-oxide nuclei that non-react and react with metal (or substrate), respectively. This is called heterogeneous nucleation. The non-reactive nucleation as seen in Fig. 7 (a) can be considered as the cluster of radius R_1 and contact angle θ_1 forming on a non-reactive substrate. In contrast, reactive nucleation as seen in Fig. 7 (b) can be considered as a double cap-shaped cluster with the upper cap having radius R_1 and contact angle θ_1, and the bottom cap having radius R_2 and contact angle θ_2. Similar to spherical homogenous nucleation, ΔG^*_N for heterogenous nucleation can be derived and given by

$$\Delta G_N^* = \frac{(16/3)\pi\gamma_f^3}{(\Delta G^0)^2} f(\theta_1) \tag{38}$$

and

$$\Delta G_N^* = \frac{(16/3)\pi\gamma_f^3}{\Delta G_0^2} h(\theta_1, \theta_2) \tag{39}$$

, for the non-reactive and reactive nucleation (Zhou, 2009), respectively. Where $f(\theta)$ and $h(\theta_1, \theta_2)$ normally called "shape factor" and given by

$$f(\theta) = \frac{(2+\cos\theta)(1-\cos\theta)^2}{4} \tag{40}$$

and

$$h(\theta_1, \theta_2) = \frac{\chi}{\chi - 1}\left(\frac{\chi - 1}{\chi} + \frac{\sin\theta_2}{\chi \sin\theta_1} \bullet \frac{\gamma_{sf}}{\gamma_f}\right)^3 f(\theta_1) \tag{41}$$

where χ is the volume ratio between the metal and oxide. The volume ratio χ can be related to the Pilling–Bedworth ratio, $\chi = Vox/Vm$, where Vm and Vox are the molar volume of the metal and oxide, respectively (Zhou, 2009). It should be noted that althought ΔG_N^* for heterogenous nucleation have a function of shape factor, the characterisic curve is not different compared with the spherical homogeneous nucleation. The shape factor just describes the magnitude decreasing of energy barrier ΔG_N^*.

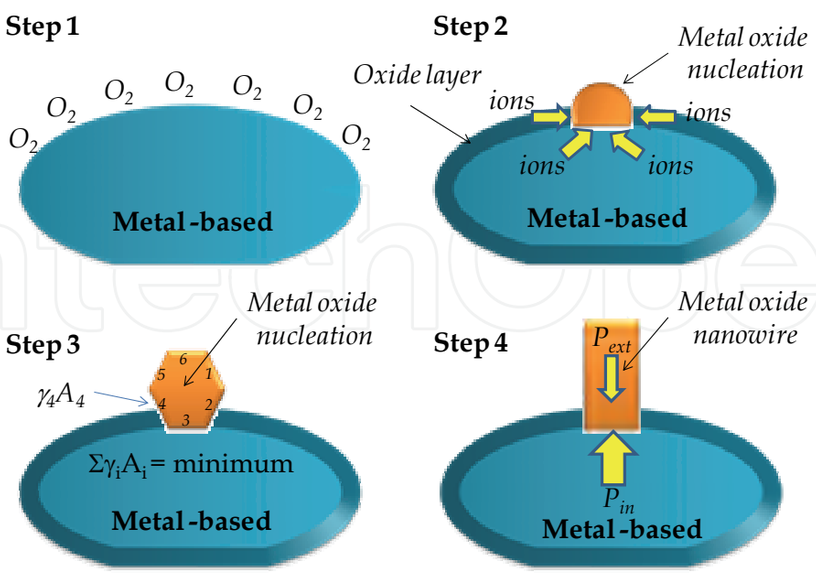

Fig. 8. Four steps of metal-oxide nanowire growth mechanism, Step 1 - oxygen adsorption, Step 2 - surface oxidization to form nuclei, Step 3 - nuclei arrangement and finally, Step 4 – nanowire formation.

Step 3. nuclei arrangement: the metal-oxide nuclei arrangement was designed based on the nuclei probability in term of the minimization of surface energy. As discuss above, a nucleation will form when it can overcome the maximum energy barrier, ΔG_N^* . Thus, we can write the probability of nucleation, P_N, and given

$$P_N = \frac{N}{N_0} = \exp(-\Delta G_N^* / k_B T) \tag{42}$$

where N is the surface concentration of nuclei and N_0 is the possible surface concentration of nuclei on metal surface, k_B is Boltzmann constant and T is temperature. It can be seen that the magnitude of P_N depends on three parameters; temperature, surface energy, and ΔG^0.

For temperature effect, it can be seen that the probability increases when the temperature increases at constant surface energy and ΔG^0. The increment of nucleation probability suggests that the nucleation frequency of formation is increased as seen in Fig 9 (a). Compare to experimental results by varying the temperatures of oxidation process, the ZnO nanowires were started to observe for heating temperature of 400°C (Fig. 9 (b)), and a lot of nanowires were observed for heating temperature of 500-800°C (Fig. 9 (c)-(f)). However, the nanowires could not be observed for heating temperature of 900°C (Fig. 9(g)). It was also found that the diameter of nanowire and the length was highest at 600°C. Therefore, the number of nanowires can be explained in term of nucleation frequency.

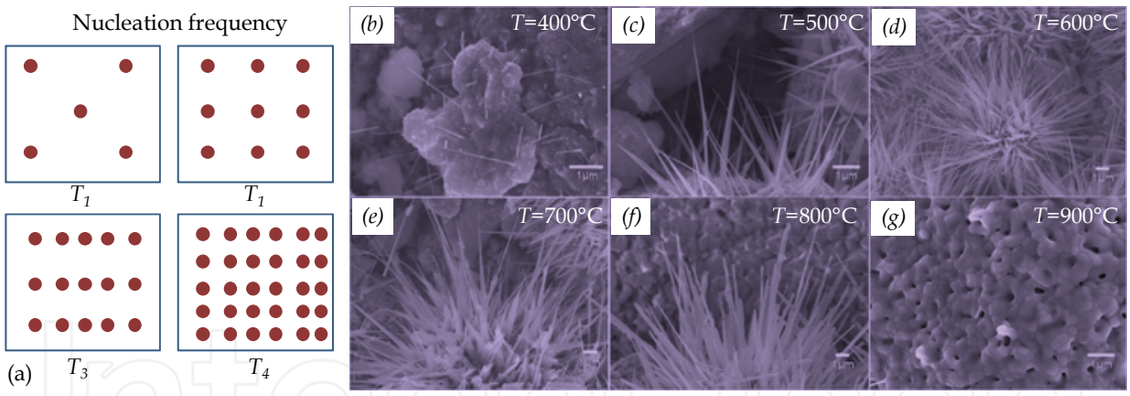

Fig. 9. (a) The increase of nucleation frequency of formation at higher temperature and (b)-(g) FE-SEM images of ZnO nanowires at various oxidation temperatures.

Structure	Example	Low-γ facets
Body-centered cubic (bcc)	Cr, Fe	{110}
Face-centered cubic (fcc)	Au, Al	{111}
Hexagonal close-packed (hcp)	Zn, ZnO, Mg	{0001}
Diamond	Si, Ge	{111}
Zinc blende	GaAs, ZnSe	{110}
Fluorite	MgF_2, CaF_2	{111}
Rock salt	NaCl, PbTe	{100}

Table 2. Facets of the lowest surface energy for various crytal structures (Smith, 1995).

After the metal-oxide nuclei was formed, the arrangement of nuclei will try to adjust itself to maximize nucleation probability or to minimize total surface energy that is

$$\sum \gamma_i A_i = \text{minimum} \tag{43}$$

Subscript i denotes terms corresponding to the nucleation free surface, the interface to the substrate, and the substrate free surface, respectively. In the case of liquid or amorphous nuclei, which have no γ anisotropy, there is only one term of $\gamma_f A_f$. In the common case of crystalline nuclei, these surface terms include all of the various exposed atomic planes or facets. So, the metal-oxide nuclei arrangement must be designed based on the high nuclei probability or low total surface energy. For example, the facets of lowest surface energy for various crystal structures are shown in Table 2.

For our work, we have specified that γ of ZnO on the {0001}, $\{11\bar{2}0\}$ and $\{10\bar{1}0\}$ is about 1.2 J/m^2, 1.4 J/m^2 and 1.6 J/m^2, respectively (Jiang et al., 2002). Therefore, the nucleation arrangement will just control the growth direction of metal nanowire. It can be seen that the growth direction of nanowires, both ZnO and CuO, has a few directions which have low miller index due to the lowest surface energy.

Step 4. **nanowire formation:** nanowire was grown by the driving force from the difference of the surface pressure between metal-oxide nucleation and substrate (or metal based). First, let consider the pressure inside the particles, which have radius r and surface energy γ as given by Laplace equation (Stolen et al., 2004) as

$$P_i = P_g + \frac{2\gamma_i}{r_i} \tag{44}$$

where P_g is the external pressure in the surrounding, subscript i referred to the solid or liquid phase. We will now consider a case where metal-oxide nucleation as a solid phase with radius r_f adsorbs on metal-based substrate with radius r_l. At interface between metal-oxide nucleation and substrate, which has surface energy γ_{sf}, the different pressure at interface is

$$P_s - P_l = \frac{2\gamma_s}{r_s} - \frac{2\gamma_l}{r_l} \tag{45}$$

In our case, we assumed that the substrate or metal-based has a large radius r_l, so the second term in Eq. 45 should be neglected. Therefore, we can write the differential form of Eq. 45 as

$$d\left(P_s - P\right)_l = d\left(\frac{2\gamma_{sf}}{r_s}\right) \tag{46}$$

Integrating from a flat interface ($r = \infty$), we obtained

$$\Delta P = P_s - P_l = \left(\frac{2\gamma_{sf}}{r_s}\right)\Bigg|_{r_s=\infty}^{r_s=r_s} = \left(\frac{2\gamma_{sf}}{r_s}\right) \tag{47}$$

It can be seen that the different pressure is inversely propotional to nucleation radius at certain surface. As an example, the different pressure at interface between the metal surface and nucleation surface is plotted as a function of the nucleation radius for a case of ZnO in Fig. 10 by using surface energy of about 1.2 J/m^2.

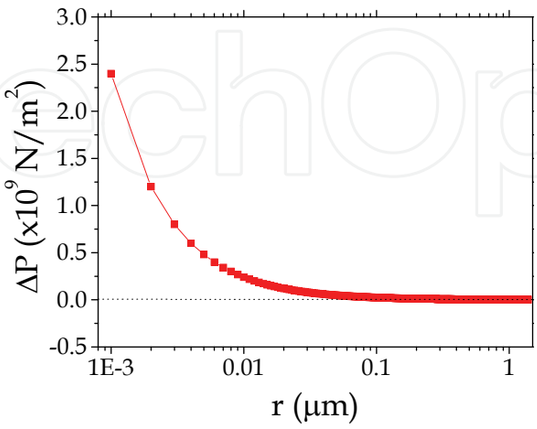

Fig. 10. Plot of the different pressure at interface between the metal surface and nucleation surface as a function of the nucleation radius for a case of ZnO.

Typically, pressure can be related to force. Thus, the increasing of different pressure at the interface suggests that there is an increasing of driving force with decreasing of the size of nucleation in order to push metal-oxide out to form nanowire. Moreover, the driving force begins to increase rapidly when the size of nucleation below 100 nm.

In the case of ZnO, at oxidation temperature of 600°C that over the melting point of Zn, oxygen molecules in air is dissociated and then adsorbed on the surface of Zn melt for ready to oxidized as discuss in Step 1. After that, the nucleation of ZnO was formed on the metal surface by the coalescence behavior of oxygen ions and metal ions. The nucleation probability depends on the temperature, surface energy and ΔG^0 as discussed in Step 2. And next step, to minimize total surface energy, the arrangement of ZnO nuclei was designed based on the nuclei probability in term of surface energy. The high possible of arrangement of ZnO nuclei is <0001>, $<11\bar{2}0>$ and $<10\bar{1}0>$ direction for their surface energy about of 1.2 J/m^2, 1.4 J/m^2 and 1.6 J/m^2, respectively (Jiang et al., 2002). Finally, the size of ZnO nucleation will be control and/or produce the driving force for nanowire growth based on the Laplace different pressure at interface between the ZnO nucleation and substrate. Since at below 100 nm the driving force increases rapidly, it can be related to FE-SEM image of ZnO nanowires that shows the size or diameter ranging in 100-200 nm. However, when the oxidation temperature is high (more than 800°C), the probability of nucleation is high too resulting in the high surface density of ZnO nuclei. Therefore, the size of nucleation is larger and there is no driving force at interface for nanowire growth.

However, CuO case is different from ZnO case because the oxidation temperature of 600°C is significantly lower the melting point of Cu metal. First, the Cu was easily oxidized to form Cu_2O layer due to the Cu_2O has lower oxidization Gibb free energy than CuO as showed in Fig 11. So, we will consider the Cu_2O as the substrate for creation CuO nucleation. Similar to ZnO case, the CuO nuclei were formed and arranged based on the minimization of total

surface energy. After that, the driving force for CuO nanowires was produced by the small size of CuO nucleation. The growth mechanism is confirmed by the cross-section FE-SEM image of CuO nanowire on Cu substrate as shown in Fig. 11. It can be seen that the thick Cu_2O layer is firstly formed on copper plate, followed by the formation of CuO layer and then CuO nanowires was finally formed on CuO layer.

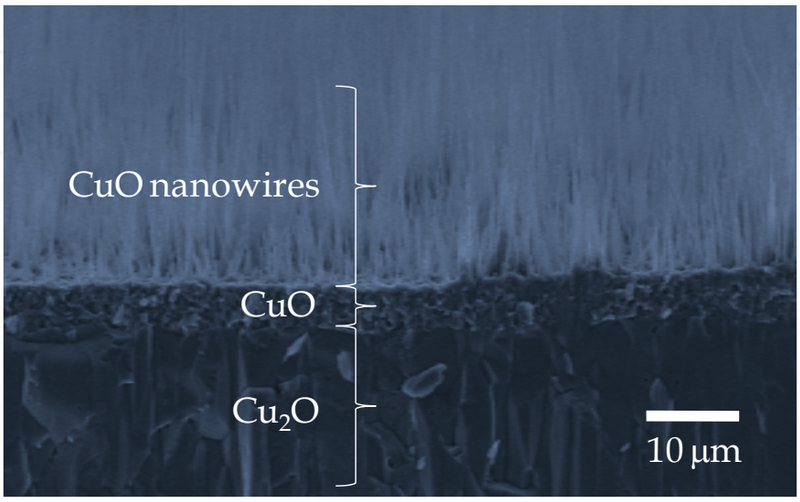

Fig. 11. Cross section FE-SEM image of CuO nanowires by heating copper plate at 600°C. Three layers can be observed for Cu_2O, CuO and CuO nanowires, respectively.

8. Applications device based on Metal-oxide nanowires

Metal-oxide nanowires are already widely used and indeed a key element in many industrial manufacturing processes. Recently, ZnO nanowires and CuO nanowires can be successfully applied as gas sensor and dye-sensitized solar cell (DSSC) (Choopun et al., 2009, Raksa et al., 2009). There are several reports that gas sensors and DSSC based on ZnO and CuO nanowire exhibited better performance than that of bulk material. For example, For gas sensor applications, normally, sensor response or the sensitivity of sensor strongly depends on the surface morphology of sensor material. From our report, nanowires were prepared by thermal oxidation of Zn powder on alumina substrate under normal atmosphere at various temperature. From sensor results, it was found that the sensitivity of nanowires sensor is improved compared with bulk sample (Wongrat et al., 2009).

9. Conclusions

This article reviews the metal-oxide nanowires among the group of ZnO and CuO which have been successfully synthesized by thermal oxidation technique. In addition, we have proposed a possible growth mechanism that may occur in the formation of nanowire. The growth mechanism can be explained in term of the Gibb free energy of oxidization process. Four steps of growth mechanism was proposed and discussed including oxygen adsorption, surface oxidization to form nuclei, nuclei arrangement and nanowire formation is considered. This growth model can be explored to explain other metal-oxide.

10. Acknowledgments

This work was supported by Thailand Research Fund (TRF). Also, we would like to thank P. Raksa, Department of Physics and Materials Science, Chiang Mai University for useful discussion on the parts of CuO nanowires. N. Hongsith would like to acknowledge the Development and Promotion of Science and Technology Talents Project (DPST) scholarship and E. Wongrat would like to acknowledge the Graduate School, Chiang Mai University for financial support.

11. References

Barsoum, M.W. (2003). *Fundamentals of ceramics*, IOP Publishing Ltd, ISBN 0-7503-0902-4, Institute of Physics Publishing Bristol and Philadelphia.

Belousov, V.V. (2007). Mechanisms of Accelerated Oxidation of Copper in the Presence of Molten Oxides. *Oxid. Met.,* 67, 235-250, ISSN 0030-770X.

Björk, M.T., Ohlsson, B.J., Sass, T., Persson, A.I., Thelander, C., Magnusson, M.H., Deppert, K., Wallenberg, L.R. & Samuelson, L. (2002). One-dimensional heterostructures in semiconductor nanowhiskers. *Appl. Phys. Lett.,* 80, 1058-1060, ISSN 0003-6951.

Chan, Y.F., Duan, X.F., Chan, S.K., Sou, I.K., Zhang, X.X. & Wang, N. (2003). ZnSe nanowires epitaxially growth on GaP(111) substrates by molecular-beam epitaxy. *Appl. Phys. Lett.,* 83, 2665-2667, ISSN 0003-6951.

Chen, J.T., Zhang, F., Wang, J., Zhang, G.A., Miao, B.B., Fan , X.Y., Yan, D. & Yan, P.X. (2008). CuO nanowires synthesized by thermal oxidation route. *J. Alloy. Compd.,* 454, 268-273, ISSN 0925-8388.

Choopun, S., Hongsith, N., Wongrat, E., Kamwanna, T., Singkarat, S., Mangkorntong, P. & Mangkorntong, N. (2008). Growth Kinetic and Characterization of RF-Sputtered ZnO:Al Nanostructures. *J. Am. Ceram. Soc.,* 91, 174-177, ISSN 0002-7820.

Choopun, S., Tabata, H. & Kawai, T. (2005). Self-assembly ZnO nanorods by pulsed laser deposition under argon atmosphere. *J. Crystal Growth,* 274, 167-172, ISSN 0022-0248.

Choopun, S., Tubtimtae, A., Santhaveesuk, T., Nilphai, S., Wongrat, E. & Hongsith, N. (2009). Zinc OxideNaonostructures for Applications as Ethanol Sensors and Dye-sensitized Solar Cells. *Appl. Surf. Sci.,* Article in press, ISSN 0169-4332.

Coleman, V.A. & Jagadish, C. (2006). Basic Properties and Applications of ZnO, In: *Zinc Oxide Bulk, Thin films and Nanostructures, Processing, Properties and Applications*, Jagadish, C. & Pearton, S. (Ed.), 1-20, Elsevier Limited, ISBN 0-08-044722-8, Radarweg 29 PO. Box 211, 1000 AE Amsterdam, The Netherlands.

Dai, Z. R., Pan, Z.W. & Wang, Z.L. (2003). Novel nanostructures of functional oxides synthesized by thermal evaporation. *Adv. Funct. Mater.,* 13, 9-24, ISSN 1616-301X.

Ellmer, K. & Klein, A. (2008). ZnO and Its Applications, In: *Transparent conductive ZnO: basics and applications in thin film solar cells,* Ellmer, K., Klein, A. & Rech, B., (Ed.), 1-33, Springer-Verlag Berlin Heidelberg, ISBN 3-540-73611-0, Springer Berlin Heidelberg Newyork.

Fan, H.J., Scholz, R., Kolb, F.M., & Zacharias, M. (2004). Two-dimensional dendritic ZnO nanowires from oxidation of Zn microcrystals. . *Appl. Phys. Lett.,* 85, 4142-4144, ISSN 0003-6951.

Hansen, B. J., Lu, G. & Chen, J. (2008). Direct Oxidation Growth of CuO Nanowires from Copper-Containing Substrates. *J. Nanomater.,* XXX, XXX-XXX, ISSN 1687-4110.

Henrich, V.E. & Cox, P.A. (1994). *The surface science of metal oxides*, The Press syndicate of the University of Cambridge, ISBN 0-521-44389-X, The Pitt Building, Trumpington Street, Cambridge.

Henrich, V.E. (2001). Metal oxide surfaces and interfaces: concepts and issues, In: *Oxide Surfaces*, Woodruff, D.P., (Ed.), 1-34, Elsevier Science B.V., ISBN 0-444-50745-0, Sara Burgerhartstraat 25 RO. Box 211, 1000 AE Amsterdam, The Netherlands.

Hirate, T., Sasaki, S., Li, W., Miyashita, H., Kimpara, T. & Satoh, T. (2005). Effects of laser-ablated impurity on aligned ZnO nanorods grown by chemical vapor deposition. *Thin Solid Films*, 487, 35-39, ISSN 0040-6090.

Hsueh, T.J. & Hsu, C.L. (2008). Fabrication of gas sensing devices with ZnO nanostructure by the low-temperature oxidation of zinc particles. *Sens. Actuators B.,* 131, 572-576, ISSN 0925-4005.

Jiang, X., Herricks, T. & Xia, Y. (2002). CuO Nanowires Can Be Synthesized by Heating Copper Substrates in Air. *Nano Lett.,* 2, 1333-1338, ISSN 1530-6984.

Jiang, X., Jia, C.L. & Szyszka, B. (2002). Manufacture of specific structure of aluminum-doped zinc oxide films by pattering the substrate surface. *Appl. Phys. Lett.,* 80, 3090-3092, ISSN 0003-6951.

Jie, J. S., Wang, G. Z., Han, X. H., Yu, Q., Liao, Y., Li, G. P. & Hou, J. G. (2004). Indium-Doped Zinc Oxide Nanobelts. *Chem. Phys. Lett.,* 387, 466-470, ISSN 0009-2614.

Kim, T.W., Kawazoe, T., Yamazaki, S., Ohtsu, M. & Sekiguchi, T. (2004). Low-temperature orientation-selective growth and ultraviolet emission of single-crystal ZnO nanowires. *Appl. Phys. Lett.,* 84, 3358-3360, ISSN 0003-6951.

Liang, H.Q., Pan, L.Z. & Liu, Z.J. (2008). Synthesis and photoluminescence properties of ZnO nanowires and nanorods by thermal oxidation of Zn precursors. *Mater. Lett.,* 62, 1797-1800, ISSN 0167-577X.

Lyu, S.C., Zhang, Y., Ruh, H., Lee, H.J., Shim, H.W., Suh, E.K., & Lee, C.J. (2002). Low temperature growth and photoluminescence of well-aligned zinc oxide nanowires. *Chem. Phys. Lett.,* 363, 134-138, ISSN 0009-2614.

Manmeet Kaur, Muthe, K.P., Despande, S.K., Shipra Choudhury, Singh, J.B., Neetika Verma, Gupta, S.K. & Yakhmi, J.V. (2006). Growth and branching of CuO nanowires by thermal oxidation of copper. *J. Crystal Growth,* 289, 670-675, ISSN 0022-0248.

Martin, M. & Fromm, E. (1997). Low-temperature oxidation of metal surfaces. *J. Alloy. Compd.*, 258, 7-16, ISSN 0925-8388.

Nguyen, D. H., Nguyen, V. Q. & Nguyen, V. H. (2009). Facile synthesis of p-type semiconducting cupric oxide nanowires and their gas sensing properties. *Physica E,* Article in Press, ISSN 1386-9477.

Raksa, P., Gardchareon, A., Chairuangsri, T., Mangkorntong, P., Mangkorntong, N. & Choopun, S. (2009). Ethanol sensing properties of CuO nanowires prepared by an oxidation reaction. *Ceram. Int.,* 35, 649-652, ISSN 0272-8842.

Raksa, P., Nilphai, S., Gardchareon, A., Choopun, S. (2009). Copper oxide thin film and nanowire as a barrier in ZnO dye-sensitized solar cells. *Thin Solid Films*, 517, 4741-4744, ISBN 0040-6090.

Ren, S., Bai, Y.F., Jun Chen, Deng, S.Z., Xu, N.S., Wu, Q.B. & Shihe Yang (2007). Catalyst-free synthesis of ZnO nanowire arrays on zinc substrate by low temperature thermal *oxidation. Mater. Lett.,* 61, 666-670, ISSN 0167-577X.

Ronning, C., Gao, P. X., Ding, Y., Wang, Z. L. & Schwen, D. (2004). Manganese-Doped ZnO Nanobelts for Spintronics. *Appl. Phys. Lett.,* 84, 783-795, ISSN 0003-6951.

Schroeder, P., Kast, M., Halwax, E., Edtmaier, C., Bethge, O. & Brückl1, H. (2009). Morphology alterations during postsynthesis oxidation of Zn nanowires. *J. Appl. Phys.,* 105, 104307, ISSN 0021-8979.

Schubert, L., Werner, P., Zakharov, N.D., Gerth, G., Kolb, F.M., Long, L. & Gösele, U. (2004). Silicon nanowhiskers grown on <111> Si substrates by molecular-beam epitaxy. *Appl. Phys. Lett.,* 84, 4968-4970, ISSN 0003-6951.

Sekar, A., Kim, S.H., Umar, A. & Hahn, Y.B. (2005). Catalyst-free synthesis of ZnO nanowires on Si by oxidation of Zn powders. *J. Crystal Growth,* 277, 471-478, ISSN 0022-0248.

Shewmon, P. (1989). *Diffusion in solids*, A Publication of The Minerals, Metal & Materials Society, ISBN 0-87339-105-5, 420, Commonwealth Drive Warrendale, Pennsylvania.

Smith, D.L. (1995). *Thin-Film Deposition: principles and Practice*, McGraw-Hill, Inc., ISBN 0-07-058502-4, New York, USA.

Stolen, S., Grande, T. & Allan, N.L. (2004). *Chemical thermodynamics of materials Macroscopic and microscopic aspects,* John Wiley & Sons Ltd., ISBN 0-4714-9230-2, The Atrium, Southern Gate, Chichester West Sussex PO19 8SQ, England.

Wagner, C. & Grunewald, K. (1938). *Z. Phys. Chem.* (B), 40, 455, ISSN xxxx-xxxx.

Wang, N., Cai, Y. & Zhang, R.Q. (2008). Growth of nanowires. *Mater. Sci. Eng. R-Rep.,* 60, 1-51, ISSN 0927-796X.

Wongrat, E., Pimpang, P. & Choopun, S. (2009). Comparative study of ethanol sensor based on gold nanoparticles: ZnO nanostructure and gold: ZnO nanostructure. *Appl. Surf. Sci.,* Article in press, ISSN 0169-4332.

Wu, Z.H., Mei, X.Y., Kim, D., Blumin, M. & Ruda, H.E. (2002). Growth of Au-catalyzed ordered GaAs nanowire arrays by molecular-beam epitaxy. *Appl. Phys. Lett.,* 81, 5177-, ISSN 0003-6951.

Yu, W., & Pan, C. (2009). Low temperature thermal oxidation synthesis of ZnO nanoneedles and the growth mechanism. *Mater. Chem. Phys.,* 115, 74-79, ISSN 0254-0584.

Zeng, J., Xu, J., Wang, S., Tao, P. & Hua, W. (2009). Ferromagnetic behavior of copper oxide-nanowire-covered carbon fibre synthesized by thermal oxidation. *Mater. Charact.,* 60, 1068-1070, ISSN 1044-5803.

Zhou, G. (2009). Nuleation thermodynamics of oxide during metal oxidation. Appl. *Phys. Lett.,* 94, 201905, ISSN 0003-6951.

Nanowires

Edited by Paola Prete

ISBN 978-953-7619-79-4
Hard cover, 414 pages
Publisher InTech
Published online 01, February, 2010
Published in print edition February, 2010

This volume is intended to orient the reader in the fast developing field of semiconductor nanowires, by providing a series of self-contained monographs focusing on various nanowire-related topics. Each monograph serves as a short review of previous results in the literature and description of methods used in the field, as well as a summary of the authors recent achievements on the subject. Each report provides a brief sketch of the historical background behind, the physical and/or chemical principles underlying a specific nanowire fabrication/characterization technique, or the experimental/theoretical methods used to study a given nanowire property or device. Despite the diverse topics covered, the volume does appear as a unit. The writing is generally clear and precise, and the numerous illustrations provide an easier understanding of the phenomena described. The volume contains 20 Chapters covering altogether many (although not all) semiconductors of technological interest, starting with the IV-IV group compounds (SiC and SiGe), carrying on with the binary and ternary compounds of the III-V (GaAs, AlGaAs, GaSb, InAs, GaP, InP, and GaN) and II-VI (HgTe, HgCdTe) families, the metal oxides (CuO, ZnO, ZnCoO, tungsten oxide, and PbTiO3), and finishing with Bi (a semimetal).

How to reference

In order to correctly reference this scholarly work, feel free to copy and paste the following:

Supab Choopun, Niyom Hongsith and Ekasiddh Wongrat (2010). Metal-Oxide Nanowires by Thermal Oxidation Reaction Technique, Nanowires, Paola Prete (Ed.), ISBN: 978-953-7619-79-4, InTech, Available from: http://www.intechopen.com/books/nanowires/metal-oxide-nanowires-by-thermal-oxidation-reaction-technique

INTECH
open science | open minds

InTech Europe
University Campus STeP Ri
Slavka Krautzeka 83/A
51000 Rijeka, Croatia
Phone: +385 (51) 770 447
Fax: +385 (51) 686 166
www.intechopen.com

InTech China
Unit 405, Office Block, Hotel Equatorial Shanghai
No.65, Yan An Road (West), Shanghai, 200040, China
中国上海市延安西路65号上海国际贵都大饭店办公楼405单元
Phone: +86-21-62489820
Fax: +86-21-62489821

IntechOpen